Article citation info:
Lv Y. Stress and defect detection of specimens based on tag array sensing technology. Diagnostyka. 2024;25(4):2024405.
https://doi.org/10.29354/diag/193823.

DIAGNOSTYKA, 2024, Vol. 25, No. 4

e-ISSN 2449-5220
DOI: 10.29354/diag/193823

STRESS AND DEFECT DETECTION OF SPECIMENS BASED ON TAG ARRAY SENSING TECHNOLOGY

Yi LV

School of Chemical Engineering and Mechanical, Liaodong University, Dandong 118003, China
Corresponding author, e-mail: Lvyi202309@163.com

Abstract

To meet the quality and accuracy requirements of structural health detection, this study is based on the Radio Frequency Identification tag array sensing technology as the core, and designs a method for metal specimen defect detection and material bending stress assessment. The experiment shows that the root mean square error of the designed fixed frequency analysis startup power algorithm and the error result of the R-squared index in the ultra-high frequency band are at the minimum level, which is suitable for the working frequency band of metal specimen defect detection. At the same time, the accuracy and recall index values of this algorithm are relatively high, located in the range of 84.41% -90.27% and 78.17% -90.26%, respectively. The application of tag array sensing defect detection technology in the evaluation of metal defect specimens and deflection bending stress is effective, and there are significant differences in the distribution of characteristic values and power levels between healthy and defective areas, indicating a good discrimination effect. This study enriches the theoretical foundation and application practice of tag array sensing technology in the field of structural non-destructive health monitoring, facilitates comprehensive stress monitoring of structures, and improves the robustness of structural monitoring schemes.

Keywords: tag array, radio frequency identification, structural health monitoring, bending stress, defect detection

1. INTRODUCTION

With the acceleration of modernization, engineering construction projects under extreme service conditions such as high heat, cold, and erosion are gradually advancing. The harsh natural environment and frequent load actions increase the risk of deformation, cracks, corrosion, and even fracture of structural components and materials. This has caused serious damage to the stability and durability of engineering projects [1] Real time monitoring during the work cycle has become the key to ensuring the safe and reliable operation of engineering projects and equipment and facilities [2]. Nondestructive Testing (NDT) refers to the damage testing and evaluation method based on the physical reaction changes caused by structural defects, while ensuring the integrity and normal use function of the specimen structure. Common NDT techniques include ultrasonic, magnetic particle, radiographic testing, and infrared imaging techniques [3]. Ultrasonic inspection is to use the ultrasonic propagation in the medium when encountering different acoustic impedance interface reflection, refraction and the nature of the waveform conversion to detect defects within the object. Magnetic particle detection is through the magnetization of ferromagnetic materials leading to the attack on the surface of the magnetic line of force changes in the formation of visually visible magnetic traces to determine defects in the workpiece. Ray detection using X-rays, γ-rays and other rays of the penetrating and ionizing effect, through the attenuation of the ray to determine whether there are defects within the object. Infrared imaging technology type through the infrared thermal imaging camera to receive infrared radiation from the object, showing the temperature field distribution on the surface of the object to determine the object defects.

However, traditional NDT still faces challenges such as long detection cycles, difficulty in identifying defects, and high requirements for operational skills. In complex environmental conditions, it is difficult to complete real-time structural detection [4]. Structural Health Monitoring (SHM) is a monitoring technique that evaluates the integrity and safety of structures through real-time or periodic monitoring using sensing or NDT technology. This technology is suitable for system monitoring in large buildings and complex outdoor environments. Therefore, the combination of NDT and structural health testing has become an effective way to detect defects in

Received 2024-07-03; Accepted 2024-09-27; Available online 2024-10-25

equipment and facilities during their work cycle [5]. The normal operation of SHM is closely related to the performance of wireless sensor networks. The flexible, passive, and wireless transmission characteristics of Radio Frequency Identification (RFID) tag perception technology are suitable for the application of SHM. SHM based on passive RFID sensing has become a topic worthy of research and attention. Therefore, this study explores the application of RFID tag sensing technology in defect and stress assessment of specimens and materials. On the one hand, the passive RFID tag antenna is utilized to transmit wireless energy to detect the health status of the target object. On the other hand, the tag can be used to send information such as the perceived stress change and distribution back to the reader through backscatter communication to realize remote monitoring.

The main innovation of the research is reflected in the proposal of a new structural health monitoring method. Compared with the traditional RFID single-tag monitoring, the research-designed method can realize the monitoring of component stress distribution and deflection assessment through the tag array layout, which provides a new technical means for non-destructive monitoring of structural health; at the same time, it expands the theoretical research and practical application areas of RFID. The paper mainly consists of four parts, starting with a summary of SHM related technologies at home and abroad. Then, the application of RFID sensing technology in defect and stress detection is elaborated, and experimental research on defect and stress detection is conducted. Finally, the research experimental results are summarized. This study is expected to promote the application of RFID tag array sensing technology in SHM, providing a more scientific and reasonable detection method for defects in specimens and materials.

2. RELATED WORKS

With the advancement of modernization and the development of wireless communication technology and the Internet of Things (IoT), the SHM project has attracted widespread attention from society and the engineering industry. In order to further innovate and develop SHM technology, domestic and foreign scholars have conducted a series of studies on SHM related technologies and methods. The removal of hazardous materials from nuclear power plants and the decommissioning process of nuclear facilities involve the identification and monitoring of hazardous specimens and materials. Therefore, Zhao A et al. introduced IoT-RFID into the cleaning and monitoring of hazardous materials and facilities, utilizing commercially available RFID tags and machine learning technology to develop integrated sensing and communication technologies. A sensing method for passive material identification and crack monitoring had been designed to achieve long-term monitoring of insulation material properties under harsh environmental conditions. This method had high recognition accuracy for material and crack characterization [6]. Mining conveyor belts played a crucial role in conveying materials during industrial operations in mines. To avoid the risk of death and economic impact caused by conveyor belt cracks, Zohra F T et al. completed the monitoring of conveyor belt cracks based on ultra-high frequency RFID tags with digital capacitance. This method could accurately detect and identify cracks, crack direction and width, with a recognition accuracy of up to 97.2%, and could withstand interference caused by conveyor belt transportation [7]. Wireless RFID provided new prospects for SHM in the IoT era. Chen L et al. designed a novel chipless RFID strain sensing tag and introduced a scalable multi-parameter sensing strategy, proposing a low-cost detection method suitable for large mechanical structures. This method expanded the coverage of IoT in key locations of building health monitoring and could be well applied to safety assessment and damage detection of large-scale infrastructure structures [8]. The application of traditional embedded sensors is susceptible to potential structural damage limitations, in contrast the application of RFID enables wireless transmission of highly sensitive strain measurement data.Nesser H et al. detected small strains within composites based on RFID on cracked wireless strain sensors, and the experimental results showed that the method can achieve economical and non-destructive detection [9].Song Z et al. used the RFID sensor tag monitoring for earthquake scared furniture vibration to find unstable objects during vibration. The study was conducted in an 8-story building in Japan, and the results showed that RFID sensor tags can recognize earthquake-induced furniture vibrations and contribute to safe living in indoor environments [10].

The existing RFID sensors usually only detect corrosion on the surface of pipelines. To achieve internal corrosion monitoring, Wu J et al. proposed an RFID sensing method based on magnetic permeability perturbation. Direct current magnetization could cause magnetic field distortion caused by internal corrosion, leading to disturbance in the permeability of the surface skin layer. Based on the disturbance changes, monitoring of internal defects in pipelines could be achieved. The surface magnetic permeability disturbance caused by internal corrosion at different depths was different, and the feasibility of this method had been verified by pipeline design with artificial defects [11]. The noise and interference present in the sensor response affected the accurate evaluation of external shocks. Balasubramanian P et al. compared the accuracy of artificial neural networks (ANN), convolutional neural networks (CNN), and long and short-term memory networks (LSTM) in estimating impact positions in sensor responses. The average absolute error of ANN was smaller, and the robustness of

CNN was better [12]. The existing unsupervised learning was mainly applied to damage detection of simple structures or components. Eltouny K A et al. designed an unsupervised learning detection framework for large-scale structural damage detection and localization using a spatiotemporal composite auto encoder network, which could achieve accurate assessment of structural health status and damage detection and localization [13]. Svendsen B T et al. designed a novel hybrid SHM framework for bridge damage detection based on numerical simulation and experimental data. The testing had verified that this framework was suitable for any bridge structure that can obtain relevant structural damage experimental data [14]. In addition, other aspects of high performance materials have been studied more extensively.Sharma S et al. found that benzothiazole oriented aniline and alkyne can be used as efficient catalysts for cationic ruthenium [15].Om H et al. carried out a study on the machining methods of shape memory alloy materials, and proposed machining techniques based on EDM, copper tool electrodes [16]. Meanwhile, the team also carried out a study on abrasive flow machining nanofinishing methods and investigated the effect of process parameters on the material removal rate and surface roughness improvement rate of brass cylindrical parts. It was found that the number of cycles contributed the most to the surface roughness with 83.48%. The effect of extrusion pressure and particle size on surface roughness was 7.38% and 8.88% respectively [17].

In summary, there have been many studies related to SHM and NDT, and their practicality and detection advantages have also been verified. However, there is relatively little research on monitoring the stress distribution on the surface of materials through RFID tag detection. In this regard, this study selected tag array sensing technology as the research object and conducted relevant research on defect detection and stress distribution evaluation of specimens.

3. STRESS ASSESSMENT AND DEFECT DETECTION OF SPECIMENS BASED ON TAG ARRAY SENSING TECHNOLOGY

SHM technology is an important means of monitoring the materials of emerging structures or specimens, which enables real-time monitoring, dynamic management, and trend analysis of structures or materials through intelligent sensing instruments. To improve the accuracy and robustness of the tag array structure detection system and achieve stable and efficient real-time monitoring, this study focuses on specimen defect detection and material stress distribution evaluation.

3.1. Design of metal specimen defect detection method based on RFID label sensing

NDT technology refers to the method of evaluating the integrity and performance of a structure or material by detecting physical properties such as light, sound, electromagnetic, and heat inside the structure or material without damaging or damaging the structure or affecting the normal use function of the test object. SHM is a real-time monitoring and evaluation of structural completion based on NDT technology. SHM can detect and solve potential structural problems in advance, take timely maintenance, reinforcement or replacement measures, and ensure the reliability and safety of the structure [18-19].

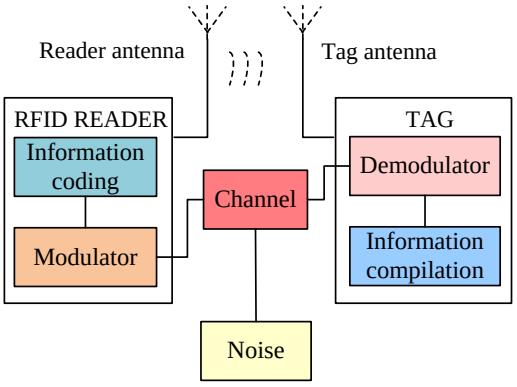

Fig. 1. Schematic diagram of RFID system structure

Structural defect detection helps to reduce the cost of component machining and improve material utilization. This study uses RFID tag sensing technology to detect defects in specimens. This technology is a wireless communication technology that recognizes and perceives electronic tags containing radio frequency signals, enabling intelligent recognition and tracking of objects. It is widely used in fields such as logistics and supply chain management, inventory management, intelligent transportation, and payment systems [20-21]. The traditional RFID system includes an RFID reader, antenna, electronic tag, and calculator control terminal, and the working mechanism is Fig. 1.

The antenna converts high-frequency current energy into electromagnetic wave energy. The basic parameters of an antenna include antenna gain, impedance, reflection coefficient, and standing wave ratio. The peak amplitude intensity is a representation of antenna gain, representing the radiation magnitude of the input power of the working circuit. The calculation process is equation (1), and P represents power. G represents antenna gain. S and U represent power density and radiation intensity, respectively. R represents the distance between the measurement point and the antenna.

$$\begin{cases} S = \dfrac{PG}{4\pi R^2} \\ U = \dfrac{PG}{4\pi} \end{cases} \tag{1}$$

The calculation process of antenna impedance Z_A is shown in equation (2). X_A and R_A respectively represent the imaginary and real parts of the antenna input impedance, namely reactance, radiation, and loss resistance. To ensure the normal use of RFID, it is usually required that the working circuit resistance is equal to the antenna resistance, and the working circuit reactance is equal to the antenna reactance.

$$Z_A = R_A + jX_A \tag{2}$$

The reflection coefficient Γ and standing wave ratio ρ of the antenna are calculated using equation (3). The ideal RFID matching state is when the standing wave ratio is $\rho = 1$.

$$\begin{cases} \Gamma = \dfrac{Z_A - Z_0}{Z_A + Z_0} \\ \rho = \dfrac{1+|\Gamma|}{1-|\Gamma|} \end{cases} \tag{3}$$

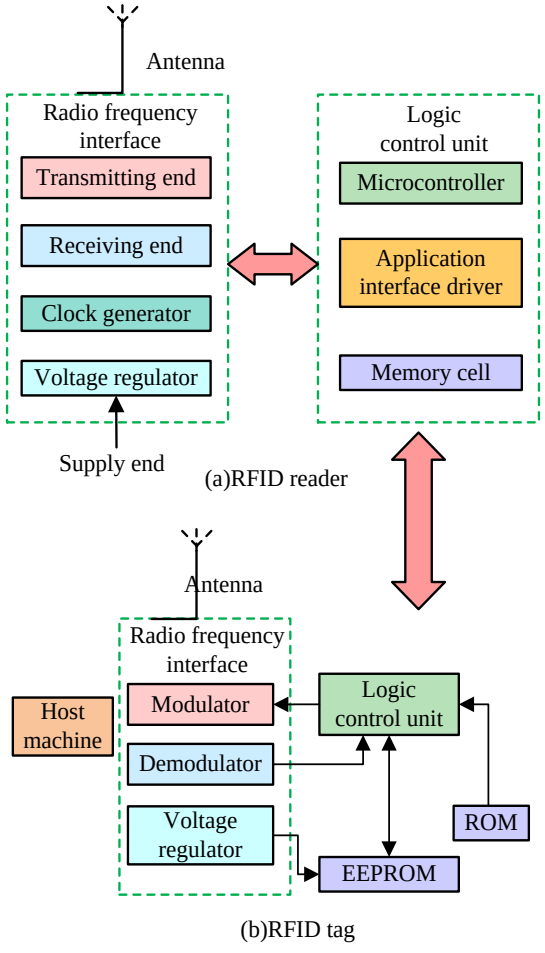

Fig. 2. Structure composition of reader and electronic tag

The reader and writer of the RFID system mainly controls the bidirectional communication of electronic tags and the connection of control instructions. Electronic tags store information negatively and complete bidirectional communication with readers and writers. The structural composition of the reader and electronic tag is Fig. 2. The logical control unit of the reader/writer is the key to RFID operation, controlling the encoding and decoding of signals as well as the identification and verification of tags [22].

Passive RFID systems include two types of systems: inductively coupled (ICP) and back-scattering coupled (BSC). The work of ICP is based on the induction field and is mainly applied to small current circuits, with certain limitations on the working distance [23-24]. The passive RFID system used in this study is a BSC type RFID system, and its circuit structure diagram is Fig. 3. The work of the BSC type RFID system is based on the radiation field, and the working frequency band is set relatively high. The power of the query signal transmitted by the reader/writer is defined as P_1, and when P_1 decays in free space and reaches the label position, the power magnitude is P_1'. The tag will absorb a portion of P_1' and convert it into the working energy of the tag IC. This absorbed energy is defined as $P_1' - P_2$, where P_2 represents the reflected power of the tag antenna. The power absorbed by the reader is processed through signal and data to obtain useful information about the label.

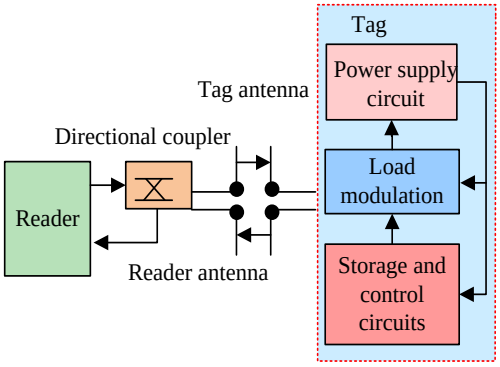

Fig. 3. BSC RFID system circuit structure diagram

The calculation process of label absorption power is equation (4). $EIRP$ represents the effective amplitude power of the antenna. G_{Tag} represents the antenna gain of the tag. λ represents wavelength.

$$P_{Tag} = \frac{\lambda^2 G_{Tag} EIRP}{(4\pi R)^2} \tag{4}$$

The calculation of label return energy is shown in equation (5). σ represents the radar scattering cross-section. P_{Reader}, G_{Reader} represent the

transmission power of the reader and the gain of the antenna, respectively.

$$P_{Tag} = \frac{P_{Reader} G_{Reader} \sigma}{4\pi R^2} \tag{5}$$

This study focuses on the detection of defects in metal specimens, using the RFID standard ISO/EPC18000. Based on the standard, the interface, protocol, and anti-collision mechanism between the reader and responder are determined. The RFID system reader for specimen defect detection is selected as the Free Real Time Operating System (FreeRTOS). FreeRTOS is developed by Richard Barry and has features such as open source code, portability, and flexible scheduling. It supports creating, deleting, and suspending tasks, assigning different priorities to tasks, and achieving communication and coordination between tasks. The FreeRTOS adopts a preemptive working mode. At the same time, to reduce the computational cost of FreeRTOS, the clock frequency is set to 500, the maximum priority level of the process is 5, the heap space size is 20K, and the minimum task stack is 128bytes. Eclipse is chosen as the development environment.

During the defect detection process of metal specimens, the characteristic values in some frequency bands may be affected by the metal specimen itself, resulting in a decrease in the reliability of the detection results. Therefore, this study considers using the method of obtaining full frequency eigenvalues to reduce the interference of the specimen itself. The purpose of the full frequency feature extraction algorithm is to enable RFID tags to extract feature values at all frequency points in the ultra-high frequency band. The full-frequency feature extraction algorithm is equivalent to the sweep algorithm in signal processing algorithms for detecting and localizing frequency components in the spectrum, which is mainly used in the fields of number processing, communications and radar. The main working idea is to change some of the frequency parameters and scan the whole signal spectrum in a specific time period. The full frequency label information extraction of the RFID RF module only requires recording the changes in the transmission power of the reader and writer. Firstly, the sweep parameters are set, and the scanning step is set to 0.5MHz; then the frequency is changed sequentially to collect the tag start power under different frequency points; finally, the localization of signal features is realized after spectrum analysis. Therefore, a Fixed Frequency Analysis Starting Power algorithm (FFASP) for RFID tag array is designed. The algorithm workflow is Fig. 4. FFASP can extract single label or multi label information, and the ratio of label return power to full frequency startup mean is used as an evaluation indicator for defect depth.

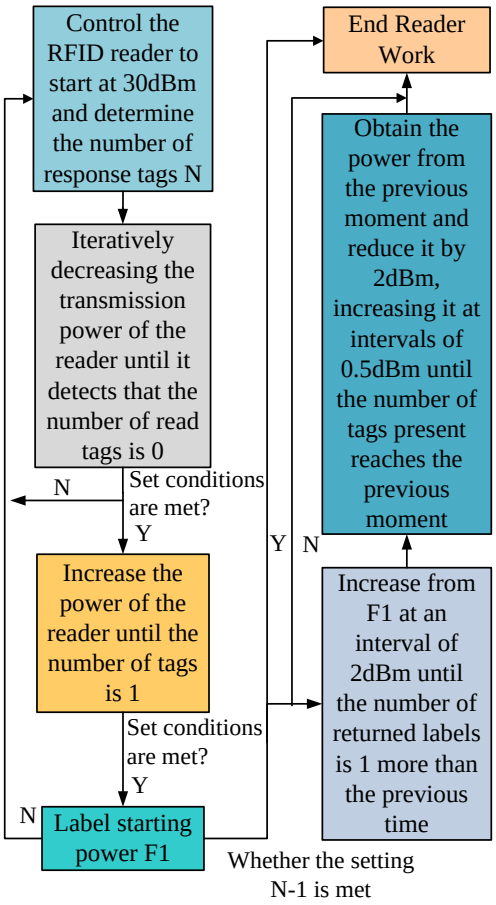

Fig. 4. RFID tag array FFASP algorithm

As seen in Figure 4, the FFAS algorithm first controls the RFID reader to start with the rated power of 30dBm, and determine the number of response tags N; then together with the iterative decreasing algorithm continuously reduces the transmit power of the reader until the readable tags for 0; then increase the power of the reader until the number of tags for 1, to get the first tag start-up power. When the set condition is not satisfied, start from the start power of the first tag and increase it every 2dBm until the number of returned tags is 1 more than the previous one, and finally get the power of the previous moment and decrease it by 2dBm, increase it by 0.5dBm intervals until the number of appearing tags reaches the level of the previous moment, and get the start power of the Nth tag. The algorithm can satisfy the information extraction of multiple tags of tag arrays to obtain the eigenvalue extraction in the ultra-high frequency band.

The RFID tag is attached to the surface of the metal specimen, and the equivalent circuit connects a metal inductor in series with the tag circuit, changing the impedance characteristics of the tag circuit and resulting in an impedance mismatch. This in turn affects the antenna performance of the tag, including its radiation efficiency, directionality, and impedance matching state, which in turn affects the minimum energy required to activate the tag, i.e., the activation power and the returned received power.

The calculation process of reflection coefficient Γ in reference equation (3) will also change the reflection coefficient of the label at the defect. Therefore, the calculation of the characteristic values defined in the study is equation (6). In equation (6), N represents the number of frequency hops. RP_f represents the received signal power. TP_f represents the transmission power of the reader/writer required to start the tag. Equation (6) can achieve one-to-one correspondence between defects and characteristic values.

$$m = \frac{1}{N}\sum_{f=902}^{928}\left(\frac{RP_f}{TP_f}\right) \tag{6}$$

3.2. Design of material stress detection and evaluation method based on RFID label sensing

To achieve long-term monitoring of material stress, the study realizes the assessment of the buckling distribution by designing a suitable label array, attaching it to the surface of the specimen and collecting the label information of the specimen under different deflections. The IMPINJ R420 fixed reader is used in this study. The electronic tag is IMPINJ H47 EPC, with a tag chip of Monza 4 and two antenna ports. The tag is divided into a tag antenna and a tag chip, as shown in Fig. 5. The complex impedance is represented as $Z_C = R_C + jX_C$ and $Z_a = R_a + jX_a$, respectively.

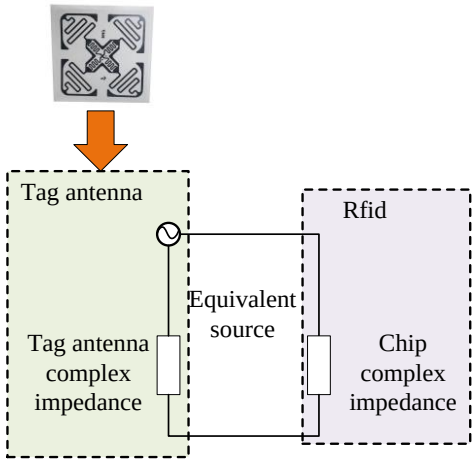

Fig. 5. Schematic diagram of IMPINJ H47 EPC label

The calculation formula for impedance matching under changes in load power is shown in equation (7). R represents the load resistance. r represents other resistors. E represents the power supply voltage. P represents the load power. The minimum power activation design of the label must meet the requirements of $X_C = -X_a$ and $R_a = R_c$.

$$P' = \frac{E^2(r-R)}{(r+R)^2} \tag{7}$$

In RFID tag sensing technology, the resonance frequency is less affected by channel fading interference, and is more sensitive to defects and antenna stretching changes. And the calculation of resonance frequency offset is relatively simple. Therefore, this study chose resonant frequency as a characterization of material curvature and defects. The calculation process of the changing resonant frequency is shown in equation (8). c represents the speed of light. L represents the geometric length of the antenna patch. ΔL represents the additional electrical length. ε represents the increase in antenna length.

$$\begin{cases} f_r' = \dfrac{c}{4(1+\varepsilon)(L+\Delta L)\sqrt{\varepsilon}} = \dfrac{f_r}{1+\varepsilon} \\ f_r' \approx f_r(1-\varepsilon) \end{cases} \tag{8}$$

At resonant frequency, the power received by the tag antenna is used to initiate the normal operation of the tag. Considering the free space propagation model adopted in the experiment, the calculation process of the received power of the tag antenna is equation (9).

$$P_{Tag} = \frac{P_{reader}G_{Tag}G_{reader}c^2}{(4\pi df)^2} \tag{9}$$

In the case of impedance mismatch, the formula for calculating the power reflection coefficient can be used to derive the relationship between the transmission power of the reader and the chip power, as shown in equation (10). The transmission power of the reader/writer can be used to determine the minimum startup power of the chip. When the operating frequency of the reader is equal to the resonant frequency of the RFID tag, the impedance matching between the tag antenna and the IC chip reaches the optimal state. Therefore, this study suggests that the lowest transmission power of the reader/writer can activate RFID tags.

$$\begin{cases} P_{chip} = P_{tag}\left(1-\Gamma^2_{tag}\right) \\ P_{reader}(f) = \dfrac{(4\pi df)^2 P_{chip}}{c^2 G_{Tag}G_{reader}\left(1-\Gamma^2_{tag}\right)} \end{cases} \tag{10}$$

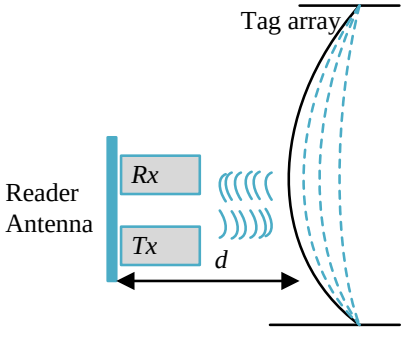

Fig. 6. Design scheme of bending deflection test experimental model

The designed bending stress assessment based on RFID sensing array has label spacing greater than 6cm, and the length and width of the test specimens are 50cm and 30cm respectively. The design scheme of the bending deflection test experimental model is

Fig. 6. During the experiment, as the deflection of the specimen increases, the deformation of the material will lead to deformation of the label and changes in the length of the label antenna. Therefore, this study sets the direction of the tag antenna port to be perpendicular to the stress direction and horizontal, respectively. During the experiment, the center and center point of the tested specimen correspond to the quarter of the horizontal and vertical axes and the endpoint. Then to operate the RFID reader to activate the tag chip by transmitting power, and the specimen stress begins to receive health monitoring from the tag array stress monitoring system. Finally, the specimen is subjected to deflection bending, and under different deflection bending conditions, the full frequency label activated power sequence is used to characterize the stress distribution. Returning the label information to the system for processing, and completing the analysis and display of monitoring data [25].

The full frequency distribution calculation of the average values of all labels with different deflections is shown in equation (11). f represents the operating frequency of the reader/writer. N_i represents the number of labels in the label array.

$$TxPower(f)' = \frac{\sum_{i=1}^{4} TxPower(f)'}{N_i} \tag{11}$$

According to equation (11), a feature value was designed to visually analyze the relationship between the returned information of the label array and the bending deflection of the specimen. The calculation process of eigenvalues is equation (12). $TxPower_i(f)$ represents the full frequency power sequence of the reader/writer activation tag. N_f represents the number of $TxPower_i(f)$ power sequences.

$$MeanPower = \frac{\sum_{i=1}^{4} \frac{\sum_{f=902}^{928} TxPower_i(f)}{N_f}}{N_i} \tag{12}$$

This study considers the information in the label array as the independent variable x and establishes a linear multiple regression model between the label array and deflection, as shown in equation (13). $\Delta(Tx)$ represents deflection. θ represents the deviation coefficient.

$$\Delta(Tx) = \theta_1 Tx_1 + \theta_2 Tx_2 + \theta_3 Tx_3 + \theta_4 Tx_4 + \theta_0 \tag{13}$$

This study uses the least squares method and gradient descent method to solve the linear regression equation. The objective function form of the least squares method is shown in equation (14), and solving the objective is to obtain θ_0 and θ_1 that make the objective function the minimum value.

$$\begin{aligned} J(\theta_0, \theta_1) &= \sum_{i=1}^{m} \left(y^i - h_\theta \left(x^{(i)} \right) \right)^2 \\ &= \sum_{i=1}^{m} \left(y^i - \theta_0 - \theta_1 x^{(i)} \right)^2 \end{aligned} \tag{14}$$

The construction of the cost function of the gradient descent method is shown in equation (15). m represents the number of points in the dataset. y represents the true coordinates of each point in the dataset. h represents the prediction function.

$$J(\theta_0, \theta_1) = \frac{1}{2m} \sum_{i=1}^{m} \left(y^i - h_0 \left(x^{(i)} \right) \right)^2 \tag{15}$$

In summary, the RFID stress monitoring system designed by the research consists of system software on the PC side as well as the RFID reader, which also contains Farsens bending sensors and an array of RFID tags. Farsens is an RFID tag developed by a Spanish company that meets international standards. Farsens impedance tags are based on a passive design that takes energy from the RF signal of the reader and sends a response signal with high accuracy and environmental adaptability.The Farsens tag used in the study is RMETER-RM, which will be used as the core component of the bending sensor to complete the construction of the bending sensor system. RMETER-RM consists of ROCKY100 IC, microcontroller and signal conditioning circuitry, with an accuracy range of 100-1, and an allowable error in the accuracy range of 1%, and a maximum measurement distance of 5m in passive mode. The overall design of the system software includes the main, parameters, data saving and hardware operation interface. The main interface consists of the hardware operation and parameter setting portals and includes help and exit options. The parameter interface provides different reader address options and sets the start and end functions for full power scanning. This interface also includes settings for step size, power and safety. In order to realize real-time and timely monitoring, the parameter setting options should include the timing function, the software through the timing function to open the reader's timer work. Hardware operation interface is mainly for RFID test and deflection test function, control IMPINJ reader hardware, test the real-time refresh; hardware operation interface is responsible for the establishment of start, disconnect and other operations with the experimental test components.

4. PERFORMANCE VERIFICATION AND EFFECTIVENESS EVALUATION OF TAG ARRAY SENSING TECHNOLOGY TESTING

To verify the effectiveness of the designed defect and stress detection methods, this study constructed testing performance verification experiments and

testing effect analysis experiments, and analyzed and discussed the results.

4.1. Algorithm performance testing of label array sensing detection scheme

For the proposed metal specimen defect detection method, the application effect of the full frequency feature extraction algorithm - FASP algorithm of the detection algorithm was evaluated first. The paper compared common feature extraction algorithms, including Principal Component Analysis (PCA), Scale invariant feature transformation (SIFT), and Accelerated Up Robust Features (SURF). To evaluate the feature extraction accuracy of FFASP algorithm, R-squared index and Root Mean Squared Error (RMSE) were selected as evaluation indicators. The experimental results are shown in Fig. 7.

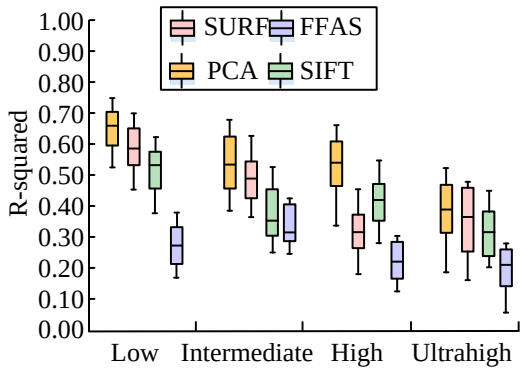

(a) R-squared

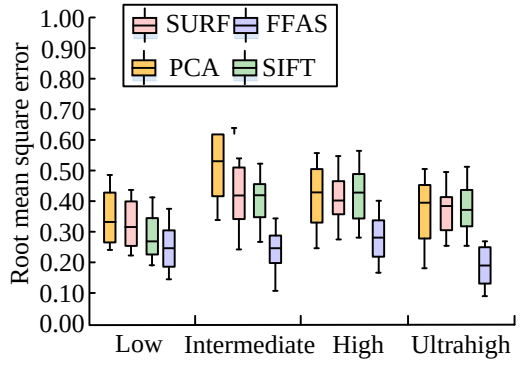

(b) Root mean square error comparison

Fig. 7. Comparison of error results of different feature extraction algorithms

The average absolute value error and RMSE both represent the magnitude of measurement error, but RMSE is greatly affected by outliers. The R-squared indicator measures the degree of fit between predicted values and true values. The experiment selected RMSE and R-squared indicators to compare the extraction errors of different feature extraction algorithms. In Fig. 7, there are significant differences in the RMSE and R-squared results of several feature extraction algorithms in different frequency bands. The evaluation values of the error indicators of the FFASP algorithm used in this study are significantly lower than the other three algorithms. The solution error of the FFASP algorithm is all below 0.40, and the error results in the ultra-high frequency band are at the minimum level, which is suitable for the working frequency band of metal specimen defect detection. Meanwhile, the R-squared indicator takes the highest value, reaching the 0.85 value level, realizing high-precision detection.

The extraction frequency of all feature extraction algorithms is set to 450, and the extraction accuracy and recall curve results of different feature extraction algorithms are shown in Fig. 8. As the number of extracted frequency points increases, the accuracy and recall curves of different algorithms fluctuate, and the range of values is relatively stable, with significant differences between the algorithms. The accuracy and recall curve of the FFAS algorithm is at the top of the coordinate axis, with an accuracy range of 84.41% -90.27% and a recall rate range of 78.17% -90.26%. The accuracy and recall of SIFT and SURF algorithms are at the bottom of the coordinate axis, respectively, and their performance evaluation results are worse than other algorithms. A higher accuracy indicates that the classifier has fewer false positives in samples with positive predictions. A high recall rate indicates that the classifier can correctly find the majority of positive examples. Usually, accuracy and recall are contradictory indicators. As shown in the test results in Fig. 8, the PCA, SIFT, and SURF algorithms did not achieve the reconciliation of conflicting indicators, but the comprehensive performance feedback of the FFASP algorithm was better.

4.2. Analysis of the effect of label array sensing defects and stress detection schemes

To select metal stainless steel specimens with artificial cracks for testing, and attach anti metal labels to the healthy areas of the specimens as well as areas with crack defects. The crack depths are 0.5, 1.0, and 1.3mm, respectively. The schematic layout of the setup for the metal crack detection experiment is shown in Fig. 9. In order to avoid the uncertainty or chance of measurement results caused by measurement errors, instrument errors and environmental factors, the final experimental structure was derived from the average of several repeated measurements and experimental calibration.

The experimental results of the minimum transmission power of the reader under normal operation of the tag and the distribution of $\frac{RP_f}{TP_f}$ at all frequencies are shown in Fig. 10. In 10 (a), at the healthy position of the specimen structure, the label startup power at full frequency is located at the bottom of the coordinate axis, with the lowest startup power. As the crack depth of the specimen increases, the starting power shows a roughly increasing trend.

Therefore, for metal specimens, the label of the healthy and defect free parts of the specimen is easier to activate. In 10 (b), the distribution of eigenvalues at the healthy position of the specimen structure is more distinct, and the distribution range of the ratio of received power to starting power is wider. The distribution of characteristic values at the defects of the specimen shows a decreasing trend as the crack depth deepens, and the ratio of received power to starting power is small.

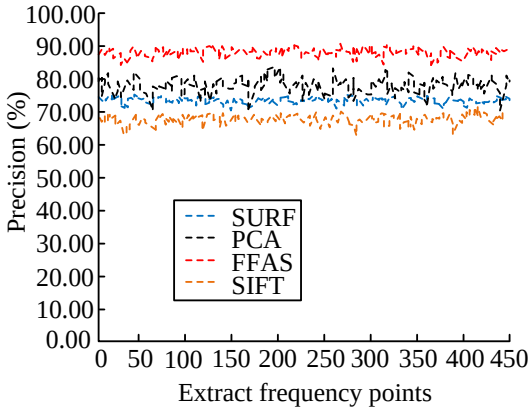

(a) Precision

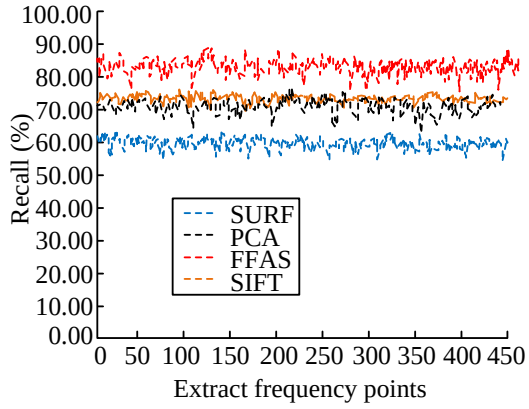

(b)Recall

Fig. 8. Performance comparison results of different feature extraction algorithms

According to the experimental design of deflection bending, labels are arranged with bending degrees set at 0, 1, 2, and 3cm respectively, and the device layout of the flexural testing experiment is shown in Fig. 11. In order to avoid the uncertainty or chance of measurement results caused by measurement errors, instrument errors and environmental factors, the final experimental structure was derived from the average of several repeated measurements and experimental calibration.

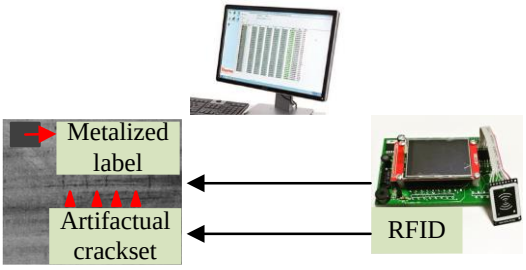

Fig. 9. Schematic layout of the device for the metal crack detection experiment

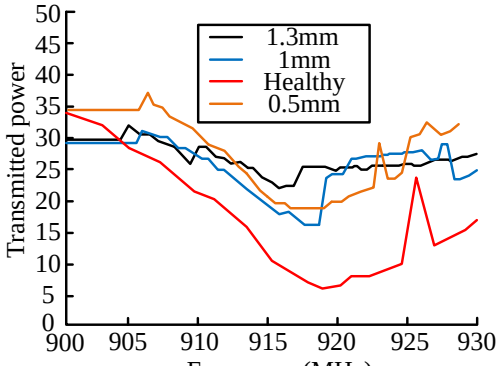

(a)Starting power

Fig. 10. Power distribution diagram of stainless steel specimens

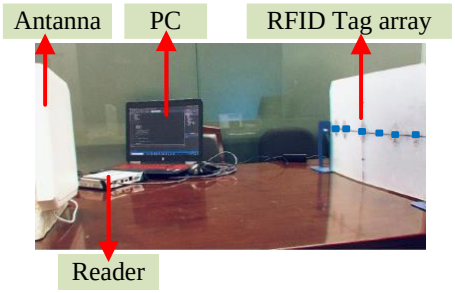

Fig. 11. Device arrangement for deflection test experiments

The deflection test results are shown in Fig. 12. The starting power distribution of the label represents the stress distribution of different specimens under different deflection sizes. As the deflection increases, the trend of the power distribution curve also increases. This is because the deflection bending changes the distance between the antenna and the tag, increasing path loss, and therefore requiring greater transmission power to activate tags with larger deflection deformation.

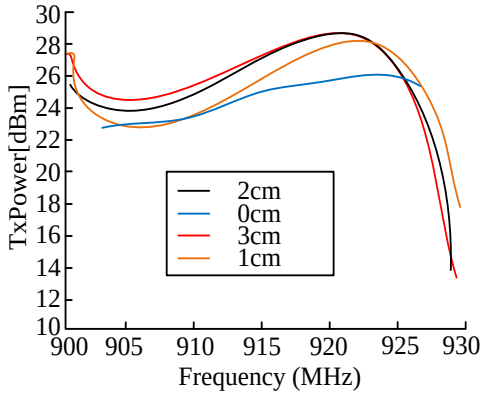

(a)Tag 1

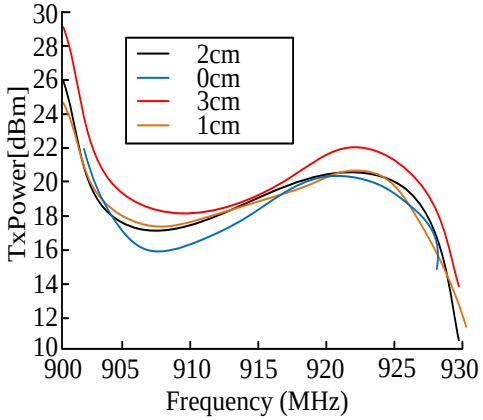

(b)Tag 2

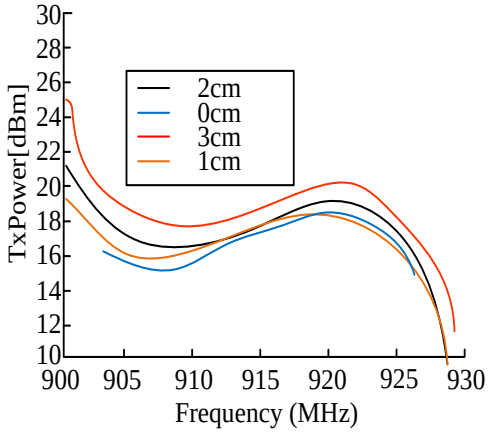

(c)Tag 3

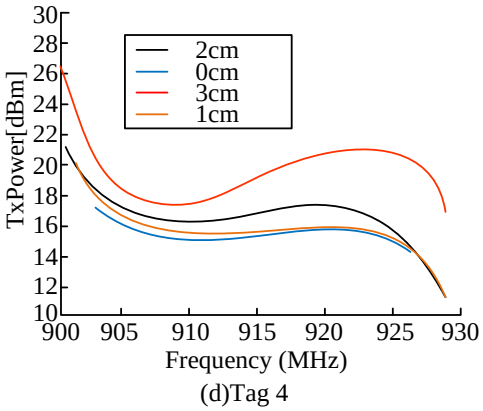

(d)Tag 4

Fig. 12. Power distribution of full frequency label startup under different deflections

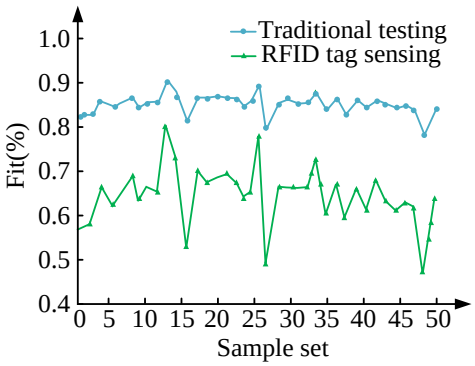

(a)Defect testing

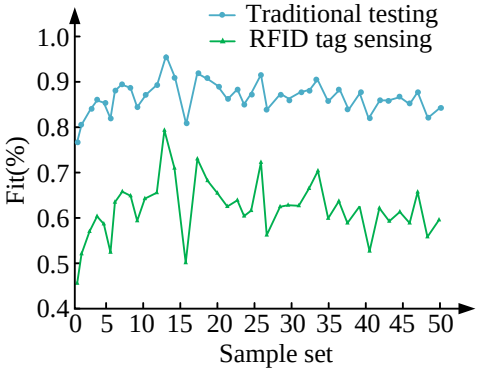

(b)Stress assessment

Fig. 13. Comparison of traditional detection and RFID label sensing detection

The evaluation results of traditional detection and RFID tag sensing detection for defects and stresses are shown in Fig. 13. Compared to traditional detection methods, RFID tag sensing detection has a higher degree of contrast and fit with real results. And the level of fit of different samples fluctuates less, with high detection stability, making it suitable for long-term stability monitoring of structures.

Table 1. Comparison of the parameters of the RFID detection scheme designed for the study

Average absolute error	
Traditional testing	Study design
0.942	0.841
Relative error	
Traditional testing	Study design
0.210	0.142
Variance	
Traditional testing	Study design
0.0956	0.0315

The test result errors were normalized, the test data significance level was set to $\alpha = 0.05$ levels, and the mean, relative error, and standard deviation of all test samples were calculated and analyzed, and confidence intervals were obtained. The results of comparing the parameters of the research-designed method with those of the traditional test are shown in Table 1. According to the confidence interval analysis, the test data in the traditional testing

method is located in the value of the confidence interval of 75%, the research design method is located in the value of the confidence interval of 95%, that is, the application of the research design of the RFID detection scheme compared to the detection accuracy increased by 20%.

5. CONCLUSION

SHM is an important component of modern large-scale buildings and infrastructure, which is related to the safety of engineering construction and people's livelihoods. This study was based on RFID tag array sensing technology as the core, and designed a method for defect detection and material bending stress assessment of metal specimens. The results showed that the R-squared and RMSE values of the FFASP algorithm were both below 0.4, and the error results in the ultra-high frequency band were at the minimum level, which was suitable for the working frequency band of metal specimen defect detection. The accuracy and recall index values of the algorithm were within the range of 84.41% -90.27% and 78.17% -90.26%, respectively. And the evaluation index results had obvious advantages. The algorithm's comprehensive performance was superior to other feature extraction algorithms. As the crack depth of the specimen increases, the starting power gradually increased. The distribution of characteristic values in the healthy part of the specimen structure was clear, and the ratio of received power to starting power was higher than that of the defect part. And as the deflect8bending increased, the trend of the transmission power distribution curve increased. Labels with larger deflection deformation required greater transmission power activation. The RFID tag sensing detection technology designed in this study has a better detection effect than traditional defect and stress detection methods, and its application effect is good. Defect detection and stress assessment using RFID tag array sensing technology can realize real-time monitoring of the target structure with higher detection efficiency and accuracy.The layout of the tag array can realize the coverage of the structure in the whole position, and discover the small defects and stress abnormalities in the structure in time.As a result, the application of RFID tag array sensing technology can build a more complete intelligent monitoring systewentm to realize the remote monitoring and intelligent management of various types of infrastructure and equipment. However, further exploration is needed on the correspondence between deflection changes and eigenvalues. In addition, there are still potential challenges and obstacles to implementing the monitoring technique designed in the study in practical applications. On the one hand, there exists the possibility of interfering with RFID signals on metal surfaces, leading to measurement errors in the start power and return signals. In complex environments, RFID signals arrive at the reader through multiple paths, leading to signal attenuation and phase changes, further affecting the accuracy of the measurements. On the other hand, there are differences in the performance of different brands and models of RFID tags, and the scalability of the technology has yet to be studied; and the cost of RFID tags, readers, and related data acquisition and processing equipment is an important issue to be considered in the field of structural monitoring.

Source of funding: *The research is supported by 2023 Dandong Guiding Science and Technology Plan (Liaodong University Joint Plan), "Research of Automotive Parts Inspection Platform Based on Computer Vision Technology", No. 10; 2024 Basic Scientific Research Project for Colleges and Universities of Liaoning Education Department, "Research on the Application of Computer Vision Technology in Mechanical Parts Inspection" [2024]No.136.*

Author contributions: *Yi Lv conducted experiments, recorded data, analyzed the results, and wrote a manuscript. Yi Lv agreed to the published version of the manuscript.*

Declaration of competing interest: *The author declares no conflict of interest.*

REFERENCES

1. Hassani S, Dackermann U. A systematic review of advanced sensor technologies for non-destructive testing and structural health monitoring. Sensors 2023; 23(4): 2204. https://doi.org/10.3390/s23042204.
2. Tan X, Chen W, Zou T, Yang J, Du B. Real-time prediction of mechanical behaviors of underwater shield tunnel structure using machine learning method based on structural health monitoring data. Journal of Rock Mechanics and Geotechnical Engineering 2023; 15(4): 886–95. https://doi.org/10.1016/j.jrmge.2022.06.015.
3. Sabato A, Dabetwar S, Kulkarni NN, Fortino G. Noncontact sensing techniques for ai-aided structural health monitoring: A systematic review. IEEE Sensors Journal 2023;23(5):4672–84. https://doi.org/10.1109/JSEN.2023.3240092.
4. Ciminello M, Sikorski B, Galasso B, Pellone L, Mercurio U, Concilio A, et al. Preliminary results of a structural health monitoring system application for real-time debonding detection on a full-scale composite spar. Sensors 2023; 23(1): 455. https://doi.org/10.3390/s23010455.
5. Yang W, Cheng X, Guo Z, Sun Q, Wang J, Wang C. Design, fabrication and applications of flexible RFID antennas based on printed electronic materials and technologies. Journal of Materials Chemistry C 2023; 11(2): 406–25. https://doi.org/10.1039/D2TC03736J.
6. Zhao A, Sunny AI, Li L, Wang T. Machine learning-based structural health monitoring using RFID for harsh environmental conditions. Electronics 2022; 11(11): 1740. https://doi.org/10.3390/electronics11111740.
7. Zohra FT, Salim O, Dey S, Masoumi H, Karmakar NC. Machine learning approach to RFID enabled health monitoring of coal mine conveyor belt. IEEE

Journal of Radio Frequency Identification 2023; 7: 105–17. https://doi.org/10.1109/JRFID.2023.3267361.
8. Chen L, Liu L, Kang L, Wan Z, Wan G, Xie L. A multibranch u-shaped tunable encoding chipless RFID strain sensor for iot sensing system. IEEE Internet of Things Journal 2023; 10(6): 5304–20. https://doi.org/10.1109/JIOT.2022.3221938.
9. Nesser H, Mahmoud HA, Lubineau G. High-sensitivity RFID sensor for structural health monitoring. Advanced Science 2023; 10(26): 2301807. https://doi.org/10.1002/advs.202301807.
10. Song Z, Rahmadya B, Sun R, Takeda S. A Feasibility study on monitoring earthquake-caused furniture vibrations using radiofrequency identification sensor tags. Sensors 2023; 23(6): 3279. https://doi.org/10.3390/s23063279.
11. Wu J, Zhang M, Liu Z, Zhang J. Magnetic permeability perturbation-based RFID sensor for pipeline internal corrosion monitoring. IEEE Transactions on Industrial Electronics 2024; 71(2): 1987–96. https://doi.org/10.1109/TIE.2023.3250747.
12. Balasubramanian P, Kaushik V, Altamimi SY, Amabili M, Alteneiji M. Comparison of neural networks based on accuracy and robustness in identifying impact location for structural health monitoring applications. Structural Health Monitoring 2023; 22(1): 417–32. https://doi.org/10.1177/14759217221098569.
13. Eltouny KA, Liang X. Large-scale structural health monitoring using composite recurrent neural networks and grid environments. Computer-Aided Civil and Infrastructure Engineering 2023; 38(3): 271–87. https://doi.org/10.1111/mice.12845.
14. Svendsen BT, Øiseth O, Frøseth GT, Rønnquist A. A hybrid structural health monitoring approach for damage detection in steel bridges under simulated environmental conditions using numerical and experimental data. Structural Health Monitoring 2023; 22(1): 540–61. https://doi.org/10.1177/14759217221098998.
15. Sharma S, Singh S, Kumari A, Sawant DM, Pardasani RT. Ruthenium-catalyzed oxidative annulation of anilines using benzothiazole as a removable directing group. Asian Journal of Organic Chemistry 2017; 6(6): 728–36. https://doi.org/10.1002/ajoc.201700098.
16. Om H, Singh S. Experimental study on electro-discharge drilling of NiTiCu10 shape memory alloy. Journal of Molecular and Engineering Materials 2024; 12(03): 2440014. https://doi.org/10.1142/S2251237324400148.
17. Om H, Singh H, Vashishtha G. An experimental investigation of process parameters on material removal and surface roughness improvement in abrasive flow machining. Engineering Research Express 2024; 6(3): 035520. https://doi.org/10.1088/2631-8695/ad63f9.
18. Silva-Campillo A, Pérez-Arribas F, Suárez-Bermejo JC. Health-monitoring systems for marine structures: A review. Sensors 2023; 23(4): 2099. https://doi.org/10.3390/s23042099.
19. Ferreira PM, Machado MA, Carvalho MS, Vidal C. Embedded sensors for structural health monitoring: Methodologies and applications review. sensors 2022; 22(21): 8320. https://doi.org/10.3390/s22218320.
20. Liu G, Wang QA, Jiao G, Dang P, Nie G, Liu Z, et al. Review of wireless RFID strain sensing technology in structural health monitoring. Sensors 2023; 23(15): 6925. https://doi.org/10.3390/s23156925.
21. Mijwil M, Kamal KH, Ruchi D, Omega JU. Advancing construction with iot and RFID technology in civil engineering: A technology review. Al-Salam Journal for Engineering and Technology 2023; 2(2):54–62. https://doi.org/10.55145/ajest.2023.02.02.007.
22. Song Z, Rahmadya B, Sun R, Takeda S. A feasibility study on monitoring earthquake-caused furniture vibrations using radiofrequency identification sensor tags. Sensors 2023; 23(6): 3279-3293.
23. John YM, Sanusi A, Yusuf I. Reliability analysis of multi-hardware–software system with failure interaction. Journal of Computational and Cognitive Engineering 2022; 2(1): 38–46. https://doi.org/10.47852/bonviewJCCE2202216.
24. Ju M, Dou Z, Li JW, Qiu X, Shen B, Zhang D, et al. Piezoelectric materials and sensors for structural health monitoring: Fundamental aspects, current status, and future perspectives. Sensors 2023; 23(1): 543. https://doi.org/10.3390/s23010543.
25. Buckley T, Ghosh B, Pakrashi V. A feature extraction & selection benchmark for structural health monitoring. Structural Health Monitoring 2023; 22(3): 2082–127. https://doi.org/10.1177/14759217221111141.

Yi LV
born in August 1973, female, Dandong, Liaoning, Han ethnicity. Graduated from Shenyang University of Technology in 1995 with a bachelor's degree in Mechanical Design and Manufacturing. Obtained a master's degree in School Education from Liaoning Normal University in 2005. Research focus: Mechatronics integration. Teacher at Liaodong University since 1995.
She has published is 2, the number of scientific research projects is 2, the number of patents is 4.
e-mail: Lvyi202309@163.com